Biomass-Directed Synthesis of 20 g High-Quality Boron Nitride Nanosheets for Thermoconductive Polymeric Composites

Xue-Bin Wang,*,†,‡ Qunhong Weng,‡ Xi Wang,‡ Xia Li,‡ Jun Zhang,‡,§ Fei Liu,*,⊥ Xiang-Fen Jiang,*,‡ Hongxuan Guo,∥ Ningsheng Xu,⊥ Dmitri Golberg,*,‡ and Yoshio Bando‡

†International Center for Young Scientists (ICYS) and ‡World Premier International Center for Materials Nanoarchitectonics (WPI-MANA), National Institute for Materials Science (NIMS), Namiki 1-1, Tsukuba, Ibaraki 305-0044, Japan, §School of Materials Science and Engineering, Hebei University of Technology, Tianjin 300130, People's Republic of China, ⊥State Key Laboratory of Optoelectronic Materials and Technologies, Guangdong Province Key Laboratory of Display Material and Technology, School of Physics and Engineering, Sun Yat-sen University, Guangzhou 510275, People's Republic of China, and ∥Global Research Center for Environment and Energy based on Nanomaterails Science (GREEN), NIMS, Sengen 1-2-1, Tsukuba, Ibaraki 305-0047, Japan

ABSTRACT Electrically insulating boron nitride (BN) nanosheets possess thermal conductivity similar to and thermal and chemical stabilities superior to those of electrically conductive graphenes. Currently the production and application of BN nanosheets are rather limited due to the complexity of the BN binary compound growth, as opposed to massive graphene production. Here we have developed the original strategy "biomass-directed on-site synthesis" toward mass production of high-crystal-quality BN nanosheets. The strikingly effective, reliable, and high-throughput (dozens of grams) synthesis is directed by diverse biomass sources through the carbothermal reduction of gaseous boron oxide species. The produced BN nanosheets are single crystalline, laterally large, and atomically thin. Additionally, they assemble themselves into the same macroscopic shapes peculiar to original biomasses. The nanosheets are further utilized for making thermoconductive and electrically insulating epoxy/BN composites with a 14-fold increase in thermal conductivity, which are envisaged to be particularly valuable for future high-performance electronic packaging materials.

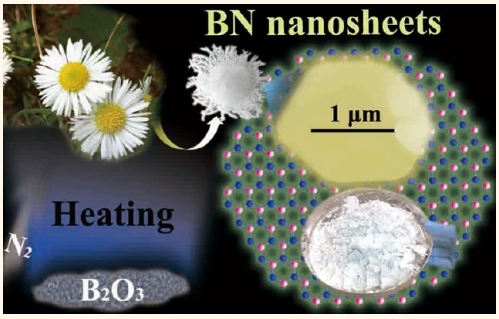

KEYWORDS: boron nitride · nanosheet · carbothermal reaction · synthesis · composite

Boron nitride (BN) nanosheets, structurally analogous to graphenes, are one of the most popular representatives of the booming two-dimensional (2D) crystals. Layered BN materials have been historically developed together with corresponding graphitic systems from fullerenes[1] *via* nanotubes[2] to nanosheets.[3] BN nanosheets are preferable over standard SiO_2 substrates for graphene-based electronics to bring exciting physics to the forefront. Ultraflat BN substrates are able to enhance the carrier mobility and to tune the band gap of graphenes.[4] BN nanosheets can either serve as high-antibreakdown dielectric gate layers or be tailored into semiconductors through doping or cutting.[3] They are also prominent spacers for tunneling devices,[5] robust protectors for graphene transistors, and good platforms for demonstrating Anderson localization,[6] Coulomb drag,[7] and strain engineering.[8] Insulating BN nanosheets are considered as the perfect companions of semimetallic graphenes. Strong in-plane and weak out-of-plane bonding further enables BN nanosheets to present a high Young modulus (~1 TPa), superb thermal conductivity (~1000 W/mK), deep-ultraviolet luminescence,[9] impressive lubrication,[10] and meaningful ion sorption[11] and hydrogen uptake.[12]

2D BN nanosheets possess higher average thermal conductivity than 0D nanoparticles and 1D nanotubes, since the two dimensionalities peculiar to the planes of nanosheets are free. Therefore, BN nanosheets are the ideal fillers for making thermoconductive polymeric composites. Currently, polymers such as epoxy, bismaleimide, and polyimide are popular electronic packaging materials,

* Address correspondence to Wangxb@fuji.waseda.jp, LIUFei@mail.sysu.edu.cn, JIANG.Xiangfen@nims.go.jp, GOLBERG.Dmitri@nims.go.jp.

Received for review May 7, 2014 and accepted August 18, 2014.

Published online August 18, 2014
10.1021/nn502486x

but they supply insufficient heat release speed due to their low thermal conductivity (0.1−0.5 W/mK). BN-nanosheet-filled polymeric composites can offer better thermal conduction while preserving the merits of insulation and easy molding of polymers. Furthermore, BN nanosheets are beneficial for the composites with respect to limiting thermal expansion and improving mechanical properties and chemical stability. The features complementary to graphene-based composites would enable their advanced applications and rival those of graphenes. BN nanosheets have been highlighted as candidates for high-performance electronic packaging, protective coatings, skincare, and functional ceramics.[13−18]

The synthesis of BN nanosheets can be traced back to the early 1990s, when epitaxial deposition was tried.[19] Recently BN monolayers/few layers have been produced *via* mechanical cleavage,[20] ball milling,[21] solution exfoliation,[13,14,22] high-energy irradiation,[23] direct reaction of boric compounds,[24,25] unwrapping nanotubes,[3] chemical vapor deposition,[26,27] substitution reaction of graphites,[28] and the reaction of boron oxide and melamine mixtures,[29] yet these methods have hardly realized the mass production of BN nanosheets. The chemical-blowing method recently developed could yield large quantities of BN nanosheets, but they exhibit rather low crystal quality.[30] The tens-of-grams production of high-quality well-structured BN nanosheets is still a great challenge.

Herein we have developed an effective and reliable biomass-directed on-site synthesis for high-throughput production of high-crystal-quality BN nanosheets. The synthesis is a variant of a carbothermal reduction reaction coupled with prevapor-transport and postnitridation processes. A throughput of *ca.* 20 g per single production run was documented. Single-crystalline, morphologically pure BN nanosheets were spatially converted just on the sites where biomass precursors had existed. They assembled in line with the original flowerlike, leaflike, or paperlike appearances. The achieved high throughput enables us to effectively utilize BN nanosheets for fabricating highly thermoconductive and electrically insulating epoxy/BN composites expected for electronic packaging.

RESULTS AND DISCUSSION

Initially, BN nanosheets were created through a separated-space reaction scheme (Figure 1a−e), in which nanosheets assembled a BN "dandelion parachute". The dandelion parachute was heated in an upper crucible upon B_2O_3 powders contained in a bottom crucible under a N_2 atmosphere at 1500 °C for producing BN nanosheets. The produced morphologically pure and thin BN nanosheets are clearly shown in Figure 1f. There were no BN byproducts such

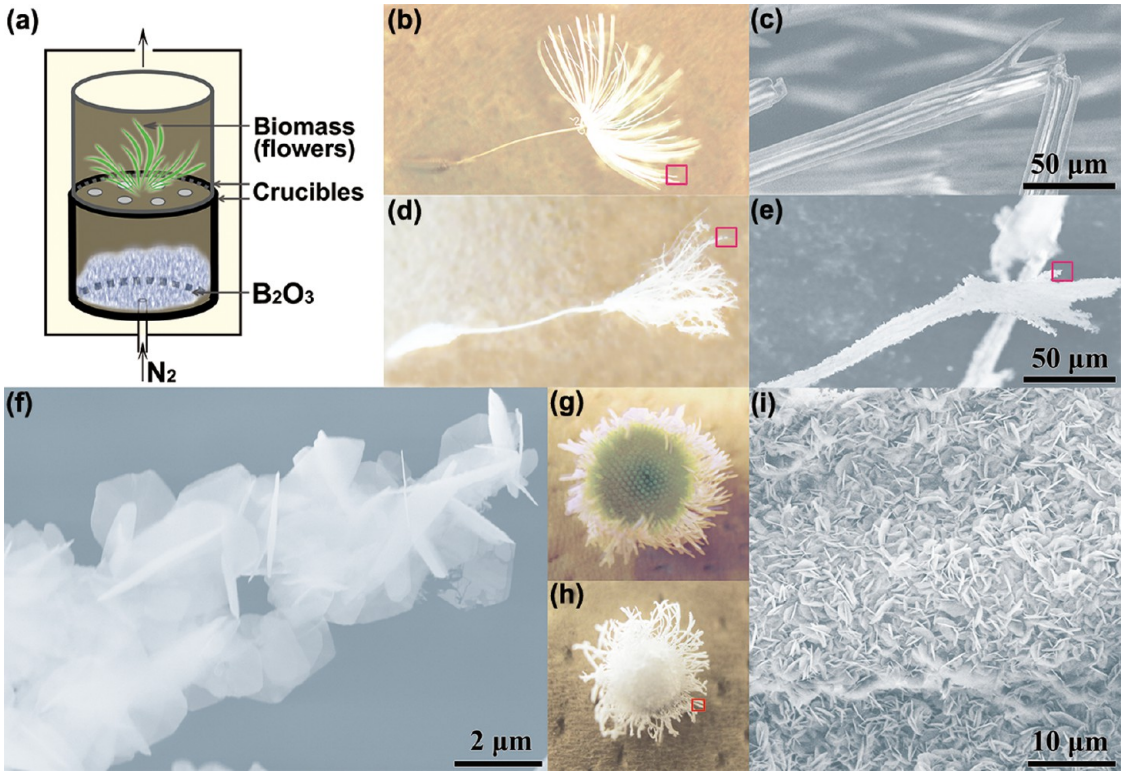

Figure 1. (a) Experimental scheme for biomass-directed on-site synthesis of BN nanosheets. (b, c) A dandelion parachute and scanning electron microscopy (SEM) image of a pappus fiber with barbs. (d, e) BN-nanosheet-assembled "dandelion parachute". (f) SEM image of a BN-nanosheet-assembled barb (taken from the marked region in (e)). (g) A fleabane flower. (h, i) BN-nanosheet-assembled "fleabane" flower and "petal".

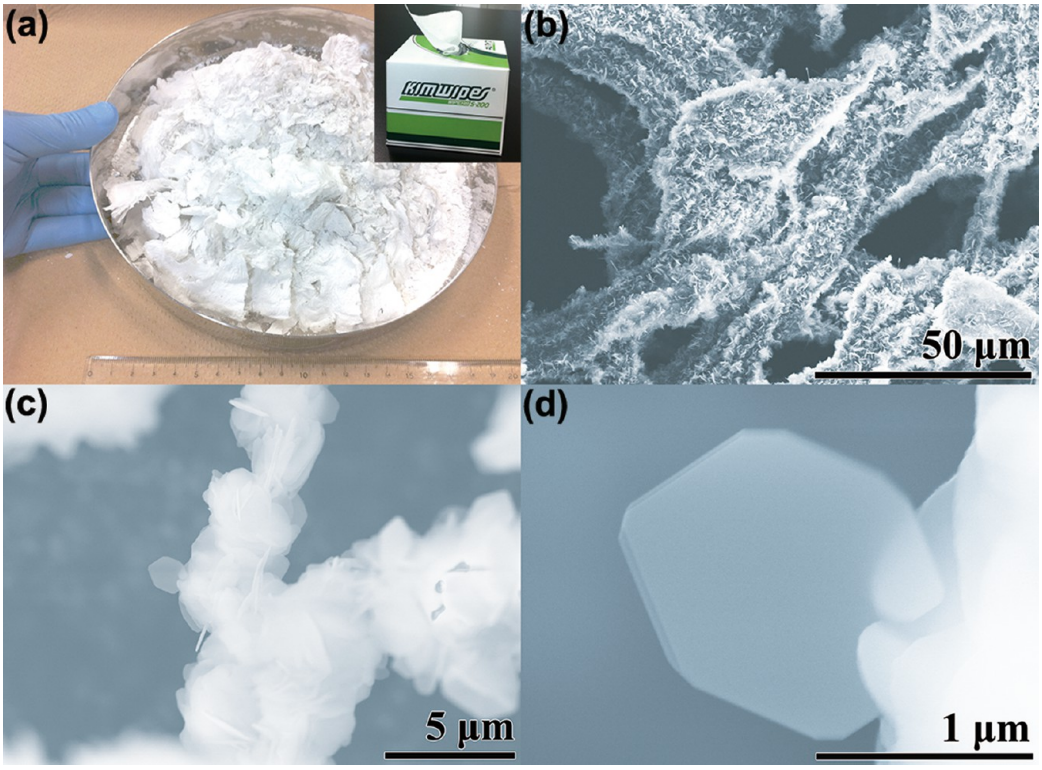

Figure 2. (a) A 20 g amount of BN nanosheets converted from wiper papers (in the inset). (b–d) SEM images of morphologically pure BN nanosheets and a nanosheet taking a truncated hexagon morphology.

as wires, rods, or tubes. The reaction occurred spatially just on the original positions/sites where the dandelion had existed, so that BN nanosheets assembled themselves to take the whole "dandelion parachute" shape with perfect copies of the achene, beak, pappi, and barbs. The copies benefit their facile transfer and may illuminate specific biomimetic potentials.

The synthesis was repeated upon the fleabane flower and pine needles to produce the BN-nanosheet-assembled "fleabane" and "pine needles", respectively, as shown in Figure 1g,h and Figure S1 (Supporting Information). Graphite could also replace the biomass for producing BN nanosheets (Figure S2, Supporting Information), but the similar process typically occurred at a higher temperature (*ca.* 1600 °C) even using graphite powders. The completely sp^2 hybridized graphite is much more stable than the biomass-derived carbon (an amorphous coke phase); thus, the biomass needs to overcome a smaller energy barrier to react with B_2O_3. Moreover, graphite might prefer a substitution reaction route at 1500 °C,[28] different from the carbothermal route discussed here for biomass. In addition, the inexpensive biomass will promote a decrease in the cost of BN nanosheets.

Large-mesh wiper papers (Figure S3, Supporting Information) were selected as a readily available carbon source for low-cost and large-scale production of BN nanosheets. A 20 g amount of snowlike BN nanosheets was successfully fabricated per single experimental run (Figure 2a–c). The nanosheets took regular morphologies of hexagons, truncated hexagons, triangles, and polygons (Figure 2d). From the statistics based on SEM images, the thickness varied from 2 to 60 nm; 23 nm was an average figure. The width of the nanosheets varied from 0.1 to 3 μm; the average value was 1 μm, which is larger than those obtained *via* a liquid exfoliation method.[13,14]

Typical truncated-hexagon-outlined BN nanosheets were further analyzed to clarify the atomic structures. The spacious nanosheet possesses only four atomic layers and perfect 150° interior angles, as shown by transmission electron microscopy (TEM) and high-resolution TEM (HRTEM) images (Figure 3a,b). The (100) fringes are clearly seen. The periodic dots in Figure 3c correspond to the honeycomb-like lattice. The BN nanosheet is a perfect single crystal, as confirmed by HRTEM (Figure 3b and Figure S4a, Supporting Information) and electron diffraction (Figure 3d). The (100) spacing is measured as 0.217(5) nm, in agreement with the standard *h*-BN lattice. The dark-field TEM also indicates the single-crystal nature without grain boundaries (Figure S4b–d, Supporting Information). Pure BN nanosheets with good crystalline quality were also characterized by Raman and infrared spectra as well as intrinsic cathodoluminescence and photoluminescence and revealed with an optical band gap of 5.6 eV (Figures S5 and S6, Supporting Information). In this BN nanosheet, the major frontier faces are symmetrically related {100} crystal planes of *ca.* 500 nm length. According to the periodic bond chain (PBC) theory,[31]

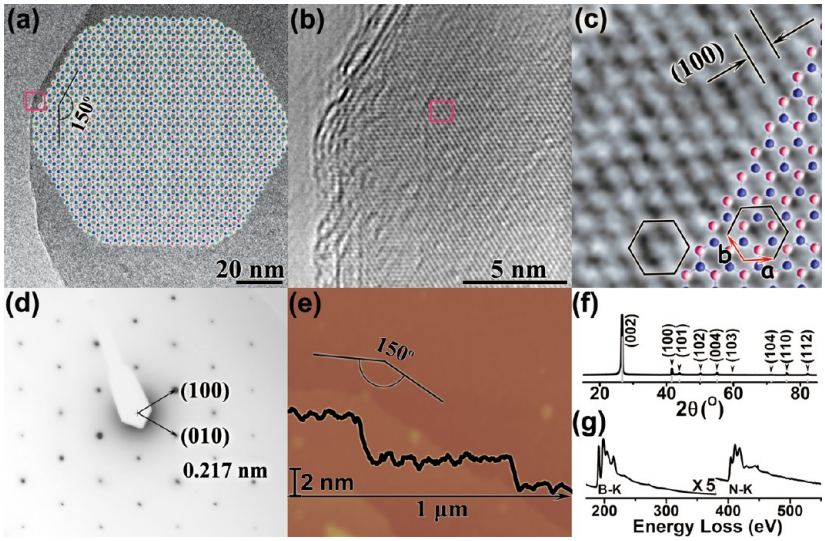

Figure 3. (a) TEM image of a truncated-hexagon BN nanosheet and its schematic structure. (b) HRTEM image taken from the marked region of (a). (c) Enlarged HRTEM image of the BN nanosheet, revealing the peculiar honeycomb lattice with basis vectors marked. (d) Electron diffraction pattern taken from a region covering the 100 nm scale domain around the two corners, oriented along the [001] zone axis. (e) AFM image and a corresponding height profile of a BN nanosheet. (f) XRD profile of BN nanosheets consistent with a standard *h*-BN. (g) EELS profile of BN nanosheets showing only characteristic B and N K-edges.

the strong PBCs are zigzag N−B−N chains parallel to the ⟨100⟩ orientation. By definition, flat {001} faces contain six interconnected PBCs which would keep themselves atomically flat, with the lowest growth speed determined by the large nucleation barrier for the new layer growth. This phenomenon constricts the thickness increase along the [001] direction and accounts for the observed thin-sheet-like morphology. Stepped {100} faces containing one PBC can grow quicker by random addition of the zigzag BN PBCs rows; thus, {100} faces are the major residual frontier sides constructing the hexagon morphology. Kinked {110} faces are predicted to be atomically rough, so that the nucleation barrier is 0, and their growth is the fastest one. The residual minor {110} frontier faces, *e.g.* the (−210) face with a *ca.* 50 nm length in Figure 3a, might be attributed to kinetic factors or local exhaustion of the growth precursors.

Atomic force microscopy (AFM) was further utilized to characterize a BN nanosheet having a 150° interior corner, as in Figure 3e. The thickness is *ca.* 2.0 nm, corresponding to six atomic layers. Layer-to-layer stacking of BN nanosheets resembles the same symmetry of the bulk sample, *i.e.* mainly AB stacking and the space group $P6_3/mmc$, as determined by X-ray diffraction (XRD) (Figure 3f). This is governed by the interlayer partially ionic attraction between neighboring layers, different from the graphene case. The ratio of crystal cell parameters *c*/*a* is 2.659, a slightly larger value than that of a standard *h*-BN (*c*/*a* = 2.658, JCPDS 340421), which implies that (002) basal plane spacing expands by *ca.* 0.04% (see Figure S7, Supporting Information). The small-size effect in thin nanosheets should account for such relaxation of basal layers. The sheetlike crystal morphology is also indicated by the broadening effect of XRD peaks, as calculated in Figure S7. The nearly stoichiometric N/B atomic ratio is determined as 1.07(6) on the basis of electron energy loss spectroscopy (EELS) characterizations of BN nanosheets (Figure 3g). The slightly higher nitrogen content probably results from the nitrogen-terminated vacancy edges formed easily in BN layers.[23,32] No carbon impurity was evidenced by EELS evaluations. Thermogravimetric (TG) analysis of the products (Figure S8, Supporting Information) confirmed that the obtained BN nanosheets contain tiny carbon impurities in the snow-white products.

The reaction process in the synthesis includes three stages: (i) a vapor transfer of B−O species, (ii) carbothermal reduction of B−O- to B-containing intermediates, and (iii) nitridation of B-intermediates to BN nanosheets (Figure 4a,b). Heating a mixture of B_2O_3 and carbon in N_2 is a traditional route to produce *h*-BN powders at 1200−1500 °C. Nevertheless, only a few studies have been performed with respect to the formation mechanism, due to the complexity of the solid-phase chemical reactions. In stage i, the gaseous B−O flow necessary for connecting two solid precursors is possibly B_2O_3(g)[33] or B_2O_2(g).[28,34] In our experiments, the B_2O_3 solid was found to become liquid and then to release a massive white smog at 1500 °C. The B_2O_3 was contained in the space separated from carbon, and it is known that the decomposition from B_2O_3 to B_2O_2 is difficult under nonreductive conditions;[35] therefore, the gaseous B−O flow is deduced to be mainly B_2O_3(g) vaporized directly, containing little gaseous B_2O_2 or B (see eq 1). This flow carried out the transfer of

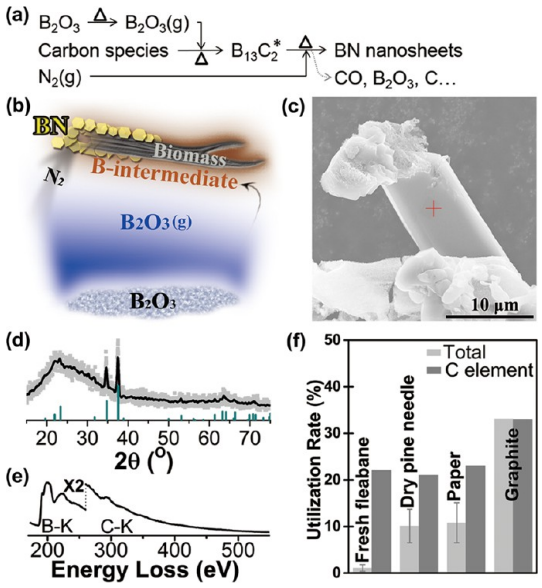

Figure 4. (a) Reaction route of heating B_2O_3 with carbon in N_2. (b) Schematic reaction mechanism of biomass-directed on-site synthesis for BN nanosheets. (c) The product through heating B_2O_3 and papers in Ar at 1500 °C. (d, e) XRD and EELS profiles of the B_2O_3-paper-Ar product (standard $B_{13}C_2$ is attached, JCPDS 330225). (f) Total and carbon element utilization rates for diverse precursors in the biomass-directed syntheses.

B_2O_3 from the bottom crucible to the upper one for producing BN.

$$B_2O_3(s) \xrightarrow{\Delta} B_2O_3(l) \xrightarrow{\Delta} B_2O_3(g) \quad (1)$$

In stage ii, the B-containing intermediate vacillates between BC_x and B in the literatures.[33,36,37] To show the B-intermediate product, we carried out a control synthesis experiment in Ar without N_2. The product was huge particles (Figure 4c and Figure S9, Supporting Information) made of a rhombohedral boron carbide crystal phase (Figure 4d). Boron carbide is a solid solution with a carbon fraction ranging from 9 to 21 atom %. Here the B/C atomic ratio was measured as 6.5(8) by EELS on dozens of samples (Figure 4e); it is denoted as B_{12}(CBC) or as $B_{13}C_2$. Obviously $B_{13}C_2$ is an easily generated phase, and it is proposed to be a possible intermediate product predominant in the reaction given by eq 2. Note that it is also possible that a B_2O_3/N_2 mixture directly reacts with carbon across other intermediates, depending on the equilibrium state of local environments.[36,37] These $B_{13}C_2$ clusters sparsely surround the carbon resources, which are further surrounded by environmental B_2O_3 and N_2. Their interfaces are the nitridation sites for forming BN nanosheets through a vapor−solid deposition (eq 3). The sheetlike BN morphology is determined by different growth speeds of crystal planes, as explained by PBC theory, while the macroscopic shape of the nanosheet ensembles is kept the same as that of the preceding carbon sources. In addition, no BN was ever seen in the case of no carbon addition. The stepped reactions are written as

$$13B_2O_3(g) + 43C(s) \xrightarrow{\Delta} 2B_{13}C_2(s)^* + 39CO(g) \quad (2)$$

$$4B_2O_3(g) + 6B_{13}C_2(s)^* + 43N_2(g) \xrightarrow{\Delta} 86BN(s) + 12CO(g) \quad (3)$$

The mechanism, as revealed by our simplified reaction scheme, is clearly different from the substitution reaction in the cases of carbon nanotubes and graphites treated with B_2O_3,[28,38] although all their total reactions are written in the form

$$B_2O_3(s) + 3C(s) + N_2(g) \xrightarrow{\Delta} 2BN(s) + 3CO(g) \quad (4)$$

In the biomass-directed synthesis, the utilization rate of carbon elements is similar for diverse carbon sources, *i.e. ca.* 20% for fresh or dry biomasses (considering water and lignocellulose to be their major contents) and *ca.* 30% for graphite, although their total conversion rates are different (Figure 4f). The utilization rate of the boron element is *ca.* 10%. Byproducts are B_2O_3 particles and carbon thin sheets deposited at cold regions (Figure S10, Supporting Information), which may be recycled in practical industrial production to improve the overall utilization rate.

The mass-produced BN nanosheets were then applied to make polymeric composites using three designed BN fractions of 1.7, 11, and 40 wt % through dispersion of BN into an epoxy resin followed by hot pressing (BN fractions were determined by TG analysis). The epoxy/BN composites look morphologically flat (Figure 5a), and no nanosheets protrude from the surface (Figure 5b). Embedded BN nanosheets were detected by spatially resolved energy dispersive spectroscopy (EDS) mapping (Figure 5c,d and Figure S11, Supporting Information). The even dispersion of fillers in the polymer matrix is the key to make decent composites. 2D nanosheets are easier to evenly disperse into composites than high-aspect-ratio 1D fillers, as seen in the 40 wt % epoxy/BN film after burning out the epoxy component (Figure 5e,f).

The performances of epoxy/BN composites were thoroughly evaluated in terms of thermal conductivity, expansion, and stability. A 40 wt % BN filled epoxy composite possesses a high thermal conductivity of 6 W/mK, *i.e.* a 14-fold increase in comparison to blank epoxy (Figure 5g). The thermal conductivity of composites shows mutational increase at *ca.* 8 wt % BN fraction, as determined by the Agari model (Figure S12, Supporting Information),[39] which corresponds to the formation of conductive networks. A conductive network together with high crystalline quality and aspect ratio of BN nanosheets contributes to the high reinforcement effect of thermal conductivity, prevailing over that using conventional fillers, *e.g.* Al_2O_3, AlN, and BN particles (Figure S12). The presented reinforcement

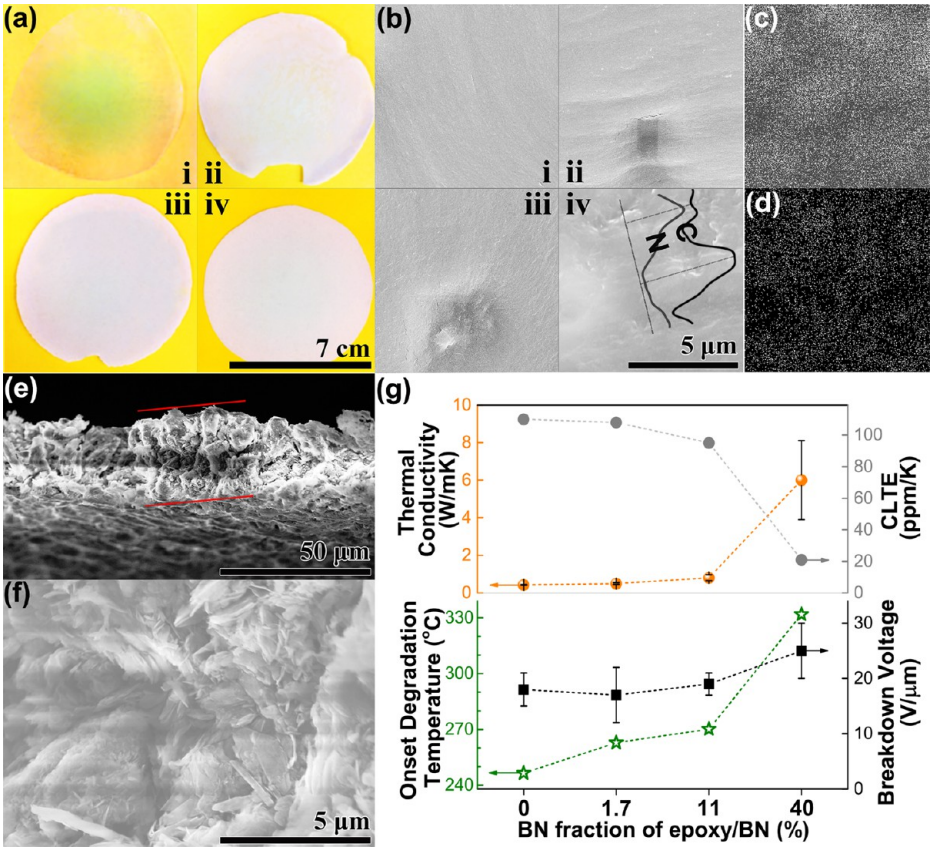

Figure 5. (a, b) Photos and top-view SEM images of blank epoxy and 1.7, 11, and 40 wt % epoxy/BN composites arranged in i–iv. The inset of (b-iv) displays EDS profiles of carbon and nitrogen elements along the marked line. (c, d) Carbon and nitrogen EDS mapping of the region of (b-iv). (e, f) Cross-sectional SEM images of the residue of the 40 wt % epoxy/BN sample after annealing in air at 600 °C, showing robust and stable BN nanosheets seen at the fracture plane. (g) Excellent performances of epoxy/BN composites with respect to heat conduction, antiexpansion, thermal stability, and antibreakdown.

effect has enabled the BN nanosheets to be fairly promising fillers.

Thermal expansion of packaging materials is demanded to match the substrates and circuits. The coefficient of linear thermal expansion (CLTE) of the composite with 40 wt % BN filling fraction is 21 ppm/K prior to the softening temperature of *ca.* 80 °C (Figure 5g). This is a value close to those of Si or Cu electronic materials and much lower than that of a blank epoxy (110 ppm/K). The constraints to the polymer chain movements by low-expansion BN (2–3 ppm/K) phase should be responsible for this effect.

The thermal durability of composites relates to their service life and safety in electronic packaging. TG analysis indicates the high thermal stability of all three composites studied (Figure 5g and Figure S13a, Supporting Information). The onset degradation temperature, defined as that corresponding to 10 wt % loss rate, increases by 85 °C after filling with a 40 wt % BN fraction. Furthermore, even after the BN part of the composites is removed in calculations, the only epoxy component demonstrates a clearly increased 10% degradation temperature (Figure S13b,c). This substantially indicates the interfacial effect of BN for the elimination of dangling bonds and radical termination of epoxy.

Epoxy/BN composites also demonstrate a low dielectric constant (Figure S14a, Supporting Information) and high breakdown fields (Figure 5g) due to the insulating nature of epoxy. This is beneficial for the reduction of parasitic capacitance in downscaling integrated circuits and crucial for preventing electrical leakage in electronic packaging. In addition, the tensile strength of epoxy/BN composites decreases with an increase in the filling fraction, but the tensile modulus is close to that of neat epoxy (Figure S14b,c). Even the epoxy composite with 40 wt % BN filling still sustains decent mechanical properties at a low density.

CONCLUSION

In summary, biomass-directed on-site synthesis has been developed for the mass production of BN nanosheets. The facile, reliable, and effective approach utilizes cheap source materials (B_2O_3, N_2, and diverse plants) to achieve morphologically pure single-crystalline BN nanosheets. The abundance of BN nanosheets enables

their applications in composites. The BN-nanosheet-filled epoxy composites demonstrate 14-fold increased thermal conductivity and are promising materials for heat release and insulating packaging.

EXPERIMENTAL SECTION

Synthesis and Characterization of BN Nanosheets. BN nanosheets were synthesized using diverse carbon sources. Any vegetation such as dandelion dispersal units (seed-bearing parachutes), fleabane flowers (erigeron annuus), and pine needles, normal wiper papers (Kimwipe S-200, Nippon Paper Crecia Co.), and graphite could serve as the carbon sources. Typically, 120 g of papers upon 350 g of B_2O_3 was heated in two detachable graphitic crucibles (total length, 30 cm; diameter, 8 cm) at 1500 °C for 5 h in an induction furnace under a N_2 flow of 2 L/min. The resultant snow-white BN nanosheet assemblies possessed the paperlike shapes and were located at the same positions where the preceding papers were placed. BN nanosheets were visualized by scanning electron microscopy (SEM, Hitachi S-4800) equipped with an energy dispersive X-ray spectrometer (EDS), high-resolution transmission electron microscopy (HRTEM, JEOL JEM-3000F), and atomic force microscopy (AFM, JEOL JSPM-5200). They were also characterized by X-ray diffraction (XRD, Rigaku Ultima III with Cu Kα radiation), electron diffraction, energy-loss spectroscopy (EELS, attachments of JEOL TEM), Raman spectroscopy (Horiba-Jovin Yvon T64000), Fourier transform infrared spectroscopy (FT-IR, Thermo Nicolet 4700), cathodoluminescence (CL, attachment of SEM Hitachi S4200), and photoluminescence (PL, Hitachi F-5700) spectroscopy.

Fabrication of Epoxy/BN Composites. Epoxy/BN composites were made using the epoxy resin polyepoxide (Araldite 506, epoxy equivalent 172-185). We used acetone as a nonreactive diluent to decrease the viscosity of the epoxy resin and to improve the dispersion of BN nanosheets. A mixture of epoxy resin (2 g) with acetone (5 g) and ratio-designed BN nanosheets was fed and stirred for 30 min. Then a curing agent, diethylenetriamine (0.2 g), was added. The resultant mixture was poured into a Teflon dish and maintained at 0 °C for 24 h to evaporate acetone, which was then kept at 20 °C for 5 h for precuring. The precured composite pieces were pressed at 40 MPa and heated to 100 °C for 2 h to complete the cross-linking reaction.

Analysis of Epoxy/BN Composites. The composite plastics were studied by thermogravimetry (TG, Rigaku Thermo plus 8120) at a 1 °C/min heating rate. The heat capacity of the composites was measured with respect to sapphire references by differential scanning calorimetry analysis at a 2 °C/min heating rate (DSC, Rigaku Thermo plus EVO 8230). Through-thickness thermal diffusivity and thermal conductivity were measured by ai-Phase Mobile 1u using a temperature-wave-analysis method according to ISO 22007-3. To measure the coefficient of linear thermal expansion (CLTE), temperature-dependent variations of composites were determined by heating rod-shaped specimens at a rate of 2 °C/min applied at a tiny load using a TMA-60 apparatus (Shimadzu Co.) in accordance with DIN 53752. Tensile tests were carried out with reference to ISO 527-2 at a rate of 0.2 mm/min using an EZ-S-100N machine (Shimadzu Co.); the elastic modulus was determined in a linear range of the stress−strain curves. The dielectric constant of composites was determined using dielectric constant analysis (Wayne Kerr precision component analyzer, West Sussex, England). The breakdown voltage of composites was measured using a dc withstand voltage tester (TW-1010DL, Tamadensoku Co.).

Conflict of Interest: The authors declare no competing financial interest.

Supporting Information Available: Figures giving the nitridized pine needles, partially nitridized graphite crucible, and raw wiper papers (SEM images), characterization of the BN nanosheets (HRTEM image, XRD, CL, PL, Raman, IR and TG analyses), characterization of the B_2O_3-paper-Ar product (EDS, TEM, and EELS analyses), and characterization of epoxy/BN composites (analyses of EDS, thermal conductivity, TG, dielectric constant, elastic modulus, breaking strength, density, and thermal capacity). This material is available free of charge *via* the Internet at http://pubs.acs.org.

Acknowledgment. The authors thank Drs. J. Tang, K. Miyano, M. Mitome, Y. Ide, A. Nukui, and N. Kawamoto, Ms. K. Takahashi, and Ms. Y. Hirai for helpful discussions and experimental assistance. This work was supported by the International Center for Young Scientists (ICYS), World Premier International (WPI) Research Center Initiative on Materials Nanoarchitectonics (MANA), National Institute for Materials Science (NIMS), KAKENHI project (Grant-in-Aid for Young Scientists, Grant Number 26820322) from the Japan Society for the Promotion of Science (JSPS), and Ministry of Education, Culture, Sports, Science & Technology (MEXT) in Japan and the National Project for the Development of Key Scientific Apparatus (2013YQ12034506) and Program for New Century Excellent Talents in University (NCET-12-0573) in the People's Republic of China.

REFERENCES AND NOTES

1. Golberg, D.; Bando, Y.; Stephan, O.; Kurashima, K. Octahedral Boron Nitride Fullerenes Formed by Electron Beam Irradiation. *Appl. Phys. Lett.* **1998**, *73*, 2441.
2. Tang, C. C.; Bando, Y.; Sato, T.; Kurashima, K. A Novel Precursor for Synthesis of Pure Boron Nitride Nanotubes. *Chem. Commun.* **2002**, *2002*, 1290–1291.
3. Zeng, H.; Zhi, C.; Zhang, Z.; Wei, X.; Wang, X.; Guo, W.; Bando, Y.; Golberg, D. White Graphenes: Boron Nitride Nanoribbons *via* Boron Nitride Nanotube Unwrapping. *Nano Lett.* **2010**, *10*, 5049–5055.
4. Dean, C. R.; Young, A. F.; Meric, I.; Lee, C.; Wang, L.; Sorgenfrei, S.; Watanabe, K.; Taniguchi, T.; Kim, P.; Shepard, K. L.; *et al.* Boron Nitride Substrates for High-Quality Graphene Electronics. *Nat. Nanotechnol.* **2010**, *5*, 722–726.
5. Britnell, L.; Gorbachev, R. V.; Jalil, R.; Belle, B. D.; Schedin, F.; Katsnelson, M. I.; Eaves, L.; Morozov, S. V.; Mayorov, A. S.; Peres, N. M. R.; *et al.* Electron Tunneling through Ultrathin Boron Nitride Crystalline Barriers. *Nano Lett.* **2012**, *12*, 1707–1710.
6. Ponomarenko, L. A.; Geim, A. K.; Zhukov, A. A.; Jalil, R.; Morozov, S. V.; Novoselov, K. S.; Grigorieva, I. V.; Hill, E. H.; Cheianov, V. V.; Fal'ko, V. I.; Watanabe, K.; *et al.* Tunable Metal-Insulator Transition in Double-Layer Graphene Heterostructures. *Nat. Phys.* **2011**, *7*, 958–961.
7. Gorbachev, R. V.; Geim, A. K.; Katsnelson, M. I.; Novoselov, K. S.; Tudorovskiy, T.; Grigorieva, I. V.; MacDonald, A. H.; Morozov, S. V.; Watanabe, K.; Taniguchi, T.; *et al.* Strong Coulomb Drag and Broken Symmetry in Double-Layer Graphene. *Nat. Phys.* **2012**, *8*, 896–901.
8. Pan, W.; Xiao, J.; Zhu, J.; Yu, C.; Zhang, G.; Ni, Z.; Watanabe, K.; Taniguchi, T.; Shi, Y.; Wang, X. Biaxial Compressive Strain Engineering in Graphene/Boron Nitride Heterostructures. *Sci. Rep.* **2012**, *2*, 893.
9. Watanabe, K.; Taniguchi, T.; Kanda, H. Direct-Bandgap Properties and Evidence for Ultraviolet Lasing of Hexagonal Boron Nitride Single Crystal. *Nat. Mater.* **2004**, *3*, 404–409.
10. Lee, C.; Li, Q.; Kalb, W.; Liu, X. Z.; Berger, H.; Carpick, R. W.; Hone, J. Frictional Characteristics of Atomically Thin Sheets. *Science* **2010**, *328*, 76–80.
11. Lei, W.; Portehault, D.; Liu, D.; Qin, S.; Chen, Y. Porous Boron Nitride Nanosheets for Effective Water Cleaning. *Nat. Commun.* **2013**, *4*, 1777.
12. Weng, Q.; Wang, X.; Zhi, C.; Bando, Y.; Golberg, D. Boron Nitride Porous Microbelts for Hydrogen Storage. *ACS Nano* **2013**, *7*, 1558–1565.
13. Zhi, C.; Bando, Y.; Tang, C.; Kuwahara, H.; Golberg, D. Large-Scale Fabrication of Boron Nitride Nanosheets and Their

Utilization in Polymeric Composites with Improved Thermal and Mechanical Properties. *Adv. Mater.* **2009**, *21*, 2889–2893.
14. Coleman, J. N.; Lotya, M.; O'Neill, A.; Bergin, S. D.; King, P. J.; Khan, U.; Young, K.; Gaucher, A.; De, S.; Smith, R. J.; Shvets, I. V.; *et al.* Two-Dimensional Nanosheets Produced by Liquid Exfoliation of Layered Materials. *Science* **2011**, *331*, 568–571.
15. Wang, X. B.; Pakdel, A.; Zhi, C. Y.; Watanabe, K.; Sekiguchi, T.; Golberg, D.; Bando, Y. High-Yield Boron Nitride Nanosheets from Chemical Blowing: Towards Practical Applications in Polymer Composites. *J. Phys: Condens. Matter.* **2012**, *24*, 314205.
16. Wang, X. B.; Pakdel, A.; Zhang, J.; Weng, Q. H.; Zhai, T. Y.; Zhi, C. Y.; Golberg, D.; Bando, Y. Large-Surface-Area BN Nanosheets and Their Utilization in Polymeric Composites with Improved Thermal and Dielectric Properties. *Nanoscale Res. Lett.* **2012**, *7*, 662.
17. Wang, X. B.; Zhi, C. Y.; Weng, Q. H.; Bando, Y.; Golberg, D. Boron Nitride Nanosheets: Novel Syntheses and Applications in Polymeric Composites. *J. Phys.: Conf. Ser.* **2013**, *471*, 012003.
18. Kiran, M. S. R. N.; Raidongia, K.; Ramamurty, U.; Rao, C. N. R. Improved Mechanical Properties of Polymer Nanocomposites Incorporating Graphene-Like BN: Dependence on the Number of BN Layers. *Scr. Mater.* **2011**, *64*, 592–595.
19. Nagashima, A.; Tejima, N.; Gamou, Y.; Kawai, T.; Oshima, C. Electronic Structure of Monolayer Hexagonal Boron Nitride Physisorbed on Metal Surfaces. *Phys. Rev. Lett.* **1995**, *75*, 3918–3921.
20. Novoselov, K. S.; Jiang, D.; Schedin, F.; Booth, T. J.; Khotkevich, V. V.; Morozov, S. V.; Geim, A. K. Two-Dimensional Atomic Crystals. *Proc. Natl. Acad. Sci. U.S.A.* **2005**, *102*, 10451–10453.
21. Li, L. H.; Chen, Y.; Cheng, B. M.; Lin, M. Y.; Chou, S. L. Photoluminescence of Boron Nitride Nanosheets Exfoliated by Ball Milling. *Appl. Phys. Lett.* **2012**, *100*, 261108.
22. Lin, Y.; Connell, J. W. Advances in 2D Boron Nitride Nanostructures: Nanosheets, Nanoribbons, Nanomeshes, and Hybrids with Graphene. *Nanoscale* **2012**, *4*, 6908–6939.
23. Jin, C.; Lin, F.; Suenaga, K.; Iijima, S. Fabrication of a Freestanding Boron Nitride Single Layer and Its Defect Assignments. *Phys. Rev. Lett.* **2009**, *102*, 195505.
24. Nag, A.; Raidongia, K.; Hembram, K. P. S. S.; Datta, R.; Waghmare, U. V.; Rao, C. N. R. Graphene Analogues of BN: Novel Synthesis and Properties. *ACS Nano* **2010**, *4*, 1539–1544.
25. Kumar, N.; Moses, K.; Pramoda, K.; Shirodkar, S. N.; Mishra, A. K.; Waghmare, U. V.; Sundaresan, A.; Rao, C. N. R. Borocarbonitrides, $B_xC_yN_z$. *J. Mater. Chem. A* **2013**, *1*, 5806–5821.
26. Ci, L.; Song, L.; Jin, C.; Jariwala, D.; Wu, D.; Li, Y.; Srivastava, A.; Wang, Z. F.; Storr, K.; Balicas, L.; *et al.* Atomic Layers of Hybridized Boron Nitride and Graphene Domains. *Nat. Mater.* **2010**, *9*, 430–435.
27. Pakdel, A.; Wang, X. B.; Bando, Y.; Golberg, D. Nonwetting White Graphene Films. *Acta Mater.* **2013**, *61*, 1266–1273.
28. Liu, F.; Mo, X. S.; Gan, H. B.; Wang, X. B.; Chen, B.; Chen, J.; Guo, T. Y.; Deng, S. Z.; Xu, N. S.; Sekiguchi, T. S.; *et al.* Cheap, Gram-Scale Fabrication of BN Nanosheets *via* Substitution Reaction of Graphite Powders and Their Use for Mechanical Reinforcement of Polymers. *Sci. Rep.* **2014**, *4*, 4211.
29. Gao, R.; Yin, L.; Wang, C.; Qi, Y.; Lun, N.; Zhang, L.; Liu, Y. X.; Kang, L.; Wang, X. F. High-Yield Synthesis of Boron Nitride Nanosheets with Strong Ultraviolet Cathodoluminescence Emission. *J. Phys. Chem. C* **2009**, *113*, 15160–15165.
30. Wang, X. B.; Zhi, C. Y.; Li, L.; Zeng, H. B.; Li, C.; Mitome, M.; Golberg, D.; Bando, Y. Chemical Blowing of Thin-Walled Bubbles: High-Throughput Fabrication of Large-Area, Few-Layered BN and C_x-BN Nanosheets. *Adv. Mater.* **2011**, *23*, 4072–4076.
31. Hartman, P.; Perdok, W. G. On the Relations between Structure and Morphology of Crystals. II. *Acta Crystallogr.* **1955**, *8*, 521–524.
32. Kotakoski, J.; Jin, C. H.; Lehtinen, O.; Suenaga, K.; Krasheninnikov, A. V. Electron Knock-on Damage in Hexagonal Boron Nitride Monolayers. *Phys. Rev. B* **2010**, *82*, 113404.
33. Aydogdu, A.; Sevinc, N. Carbothermic Formation of Boron Nitride. *J. Eur. Ceram. Soc.* **2003**, *23*, 3153–3161.
34. Joon, S. J.; Jha, A. A Vapour-Phase Reduction and the Synthesis of Boron-Based Ceramic Phases. *J. Mater. Sci.* **1995**, *30*, 607–614.
35. Kuo, K. K. Y.; Acharya, R. *Applications of Turbulent and Multi-Phase Combustion*; Wiley: Hoboken, NJ, 2012.
36. Bartnitskaya, T. S.; Kosolapova, T. Y.; Kurdyumov, A. V.; Oleinik, G. S.; Pilyankevich, A. N. Structure and Some Properties of Fine-Grained Graphite-Like Boron Nitride. *J. Less Common Met.* **1986**, *117*, 253–258.
37. Camurlu, H. E.; Sevinc, N.; Topkaya, Y. Effect of Calcium Carbonate Addition on Carbothermic Formation of Hexagonal Boron Nitride. *J. Eur. Ceram. Soc.* **2008**, *28*, 679–689.
38. Han, W.; Bando, Y.; Kurashima, K.; Sato, T. Synthesis of Boron Nitride Nanotubes from Carbon Nanotubes by a Substitution Reaction. *Appl. Phys. Lett.* **1998**, *73*, 3085.
39. Agari, Y.; Ueda, A.; Nagai, S. Thermal Conductivity of a Polymer Composite. *J. Appl. Polym. Sci.* **1993**, *49*, 1625–1634.